JOURNAL OF SOLID STATE CHEMISTRY 94, 79–88 (1991)

Symmetry of the Unoccupied States in Cs Graphite Intercalation Compounds by X-Ray Absorption

V. CODAZZI, G. LOUPIAS,* AND S. RABII†

Laboratoire de Minéralogie-Cristallographie, associé CNRS, Univ. Paris VI et VII, Tour 16, 4-place Jussieu, 75252 Paris-Cedex 05, France

L. ELANSARI AND D. GUÉRARD

Laboratoire de Chimie du Solide Minéral, associé CNRS, Univ. de Nancy I, B.P. 239, 54506 Vandoeuvre-les-Nancy Cedex, France

AND I. ASCONE*

Laboratoire de Chimie Théorique, associé CNRS, Univ. de Nancy I, B.P. 239, 54506 Vandoeuvre-les-Nancy Cedex, France

Received May 18, 1990; in revised form April 5, 1991

The X-ray photoabsorption spectra of the first three stages of cesium graphite intercalation compounds have been measured at the L absorption edges of Cs, using a linearly polarized synchrotron beam. The results are interpreted based on the self-consistent field energy band calculation for CsC_8. The L_I spectra show strong dependence on the polarization angle of the incident radiation. The structures are well correlated with the p_x, p_y, and p_z final states located on Cs sites. In L_{II} and L_{III} spectra the familiar white lines, characteristic of metals, are observed. These are attributed to transitions to unoccupied states with atomic d character at Cs sites. The results also indicate that the charge transfer between Cs and C layers in CsC_8 is nearly unity.

I. Introduction

Graphite intercalation compounds (GICs) are characterized by their layered structure and the fact that they exhibit staging phenomena, i.e., a regular stacking of n carbon layers between two intercalant sheets. The value n is referred to as the stage of the compound. Intercalants of general interest to us are alkali metals, where the intercalant atom donates part of its outer electron to the graphite layer. These are referred to as donor compounds. The present work deals, specifically, with Cs compounds.

The layered nature of these compounds often leads to particular symmetry of wavefunctions with respect to the carbon planes, at each lattice site. For example, the wavefunctions for a specific energy level, at a particular k point in the Brillouin zone, and at any lattice site contain either a mixture of

* Laboratoire d'Utilisation du Rayonnement Electromagnétique, CNRS-CEA-MEN Universite Paris-Sud bât. 209c, 91405 Orsay-Cedex, France

† Permanent address: Department of Electrical Engineering, University of Pennsylvania, Philadelphia, Pennsylvania, 19104.

0022-4596/91 $3.00

p_x and p_y atomic functions or those of p_z symmetry but not both. The Z-axis in this context is taken to be perpendicular to carbon layers (the c-axis of graphite). If the states with these different symmetries are separated in energy, one can use linearly polarized photons in X-ray absorption or emission near edge spectra to study the symmetry of the unoccupied or occupied states. For example in the K and L_I edge spectra, where the transitions start from s core levels, transitions are only allowed to states of p_x or p_y symmetry, when the electric field of the incident radiation is in the carbon plane. Furthermore, due to the fact that the core states are very localized in space, only the component of the wavefunction at a specific lattice site is probed. The site-specific nature of these measurements make them ideal for the study of hybridization of the wavefunctions and phenomena such as charge transfer between the intercalant and the carbon layers. We have already measured the absorption spectra at the K edge of potassium for GIC and interpreted it based on our energy band structure calculations (*1*). In the present study, we have measured L_I, L_{II}, and L_{III} spectra of Cs intercalation compounds as a function of polarization angle and stage. Section II of this paper describes the sample preparation and Section III the measurement techniques. Theoretical formalism used in the energy band calculations is discussed in Section IV, with the results and discussion given in Section V.

II. Sample Preparation

The low stage (n = 1 to 3) compounds were prepared by the two-zone tube method (*2*), with Cs held at 200°C and highly oriented pyrolitic graphite (HOPG) at 210, 350, and 400°C for stages 1, 2, and 3, respectively. For higher stages, a mixture of about 1 g of second stage and graphite powder is heated to about 200°C, along with the HOPG sample. The ratio of the second stage to graphite is calculated to reach the composition of a given compound at the end of the process (*3*). The stoichiometry for the first stage Cs compound as well as for K and Rb is MC_8. For the higher stages, the composition is MC_{12n}, where n is the stage of the compound.

An important parameter for the measurement is the thickness of the sample, so that a suitable amount of absorption (about 90%) occurs at the Cs edges (about 5 to 6 keV). The initial thickness of the HOPG sample varied from 20 μm (stage 1) to 140 μm (stage 8). Thicker samples are necessary as the stage increases in order to compensate for decreasing Cs concentration. With such thin samples, protection against oxidation becomes important, even though the measurements are carried out in transmission. In our first attempt, the samples were sealed in bronze cells with Kapton foil windows. Unfortunately, the cesium coming from the sample, for stages 1 and 2, was reactive enough to create holes in the Kapton foil and lead to the destruction of the samples. This happened in spite of the fact that by maintaining proper temperature gradient we had avoided the formation of free metal on the sample surface. These problems were absent in the case of K GICs. We, finally, used beryllium plates as windows. At energies corresponding to the Cs edge, the absorption due to the 200-μm thick beryllium plates is small enough to make the measurement possible.

The samples were transferred from the preparation tube to the bronze cell in a glove box under argon gas and purified by molecular sieves and titanium-zirconium chips heated to 900°C. The sample holder was sealed under argon gas. The stage of the sample was, then, confirmed by X-ray analysis.

The stacking sequence for CsC_8 is $A\alpha A\beta A\gamma$ . . . with the space group $P6_222$ (*4*). This is in contrast to the first stage K and Rb compounds which have the

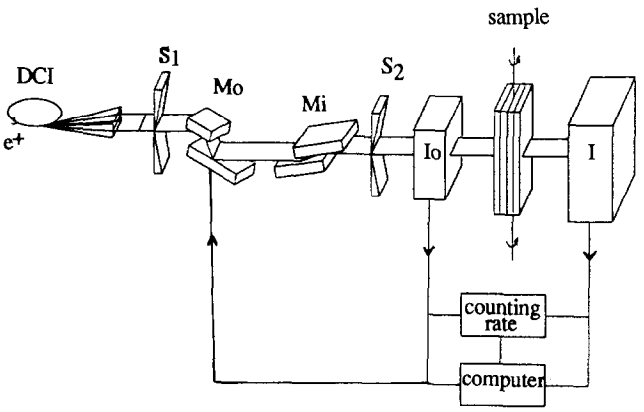

FIG. 1. Experimental setup. Slits S_1 and S_2 are 5 m apart with openings of 200 μm. The monochromator (Mo) used 311 Bragg reflections of two silicon single crystals. A double uncoated glass mirror (Mi) is used to harmonic rejection.

$A\alpha A\beta A\gamma A\delta$ . . . sequence with the space group *Fddd* (*5, 6*).

III. Measurements

The experiments were carried out at Laboratoire pour l'Utilisation du Rayonnement Electromagnétique (LURE), at EXAFS II station, using the linearly polarized synchrotron beam. A two-crystal Si(311) monochromator provides an X-ray beam tunable around the energy of the L absorption edges of cesium. The polarization ratio of the monochromatized beam is better than 99%. This high ratio is obtained by using a sharply collimated white beam coming from the central part of the photon source and a vertical scattering plane for the monochromator (Fig. 1). The polarization angle Θ is defined as the angle between the electric field **E** and the normal to the sample, i.e., the *c*-axis (Fig. 2). The angle Θ is varied between 90° and 30° in 15° steps. For each value of Θ, the spectrum of the transmitted photons through the sample is recorded in the useful energy range by 0.25-eV steps. In this Bragg reflection, the second harmonic is practically absent in the monochromatic beam. Two uncoated glass mirrors are used to reject the remaining harmonics with a rejection ratio (*7*) of 10^{-4} in this energy range (5 to 6 keV).

The experimental resolution, determined (*8*) by the openings of S_1 and S_2 slits, their separation, the distance, and the size of the source, is 0.4 eV. Thus the total resolution is dominated by the core level width (*9*), i.e., 3.78 eV for the L_I edge and 3.25 eV for the L_{III} edge.

Even though the first-stage compound CsC_8 is ordered at room temperature, all the measurements were carried out at liquid

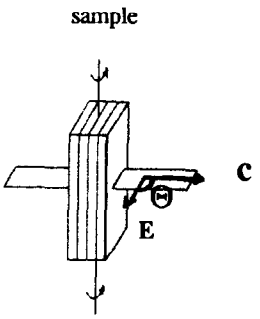

FIG. 2. Definition of polarization angle Θ.

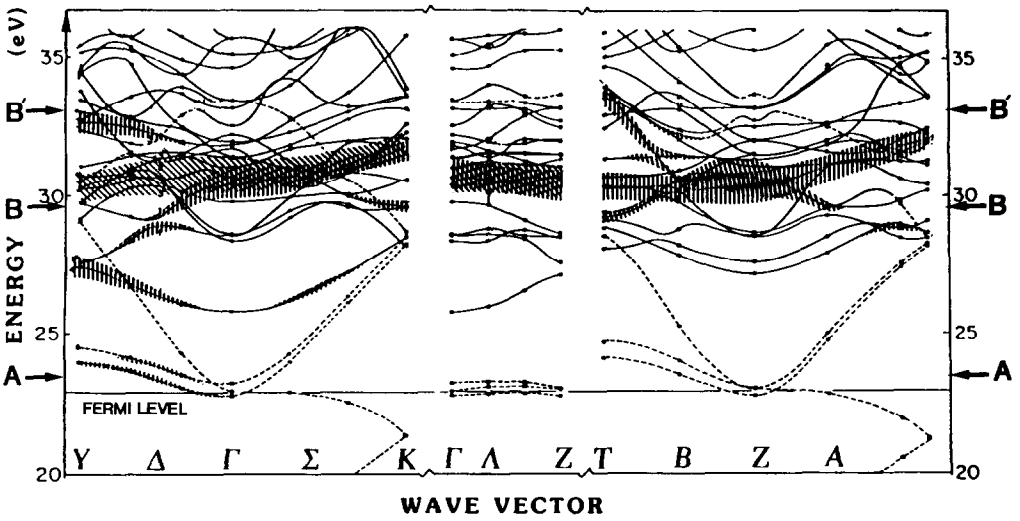

FIG. 3. Partial energy band structures of CsC_8, showing p_{xy} content of the unoccupied states at the Cs site. Heights of the shaded areas are proportional to the sum of the p_x and p_y components of the wavefunctions.

nitrogen temperature to ensure that the higher stages were also ordered (*10*).

IV. Theory

Self-consistent field (SCF) energy bands for CsC_8 (*11, 12*) were obtained within the density functional formalism (*13, 14*) using *ab initio* normconserving pseudopotentials (*15*). Since in these calculations we were interested in comparative studies of the energy band structure of all the three heavy alkali compounds, we assumed a common stacking sequence $A\alpha A\beta$ . . . with the associated space group *Fmmm'* for all. The pseudopotentials were nonlocal and included *s*, *p*, and *d* components for Cs and *s* and *p* for C. A local density approximation (*16*) was used for exchange-correlation potential. The wavefunctions were expanded in a mixed basis of plane waves and localized orbitals (*17*). The localized parts of the final wavefunctions are used to obtain information about their content and symmetry at each atomic site. The nonorthogonality of the basis makes an exact assignment of weight to the local part difficult. Nevertheless, one can relate the cesium *p* and *d* contents of the wavefunction to the corresponding coefficients in its expansion, indicating whether there is strong, weak, or no presence of a given component.

This information is shown in Figs. 3–5, referred to as *partial band structures*, for states above the Fermi level. Widths of the cross-hatched regions are proportional to the linear combination of atomic orbitals (LCAO) content of the wavefunctions at the cesium site. Figure 3 presents the results for combined Cs p_x and p_y components (hereafter referred to as p_{xy}), while Fig. 4 gives the corresponding information for Cs p_z. Since the spin-orbit splitting of the unoccupied Cs 5*d* levels is negligibly small (about 0.04 eV), the $5d_{3/2}$ and $5d_{5/2}$ levels overlap due to the band broadening. Thus, the different *d* levels do not group separately in energy. For this reason, Fig. 5 shows the partial band structure for the five different *d* orbitals combined. It should be noted that Saito and

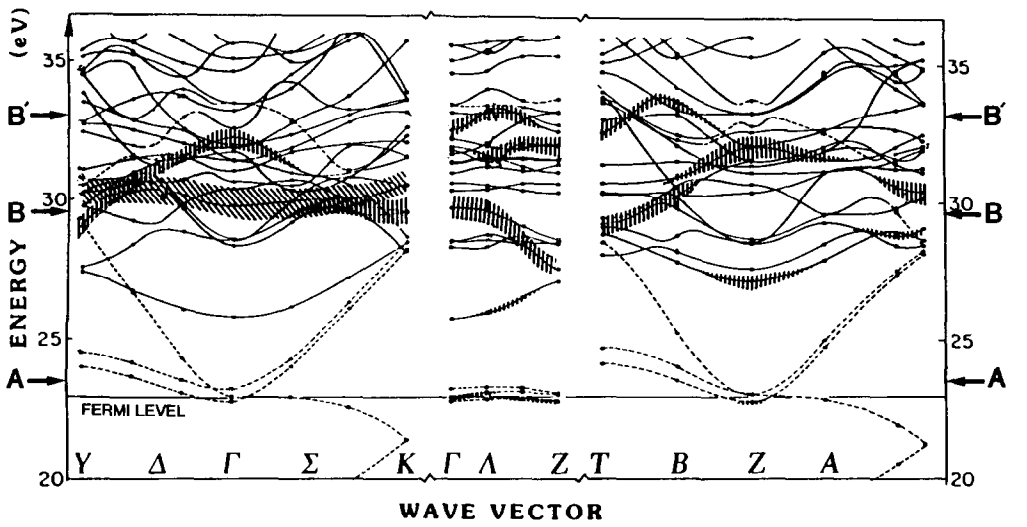

FIG. 4. Partial energy band structures of CsC_8, showing p_z content of the unoccupied states at the Cs site. Heights of the shaded areas are proportional to the p_z component of the wavefunctions.

Oshiyama (*18*) have also carried out a SCF calculation for energy band structure of CsC_8 using LCAO. Their results are very similar to ours and show a nearly complete (94%) charge transfer between the intercalant and the carbon layers.

V. Results and Discussion

A. L_I Edge

L_I edge transitions initiate from $2s$ core levels of Cs and thus the only allowed transitions are to final states with p symmetry. The wavefunctions in Cs intercalation compounds, due to their layered nature, have either p_{xy} or p_z component, but not both. Transition to final p_{xy} states is forbidden if the electric field **E** of the incident light is parallel to the c-axis of the sample ($\Theta = 0°$) and increases to its maximum for $\Theta = 90°$. The behavior for transition to final states of p_z symmetry is the opposite. Since often there exist final states of both symmetries in the same energy range, the strength of a peak varies as

$$\mu(E,\Theta) = \mu_{xy}(E) \sin^2\Theta + \mu_z(E) \cos^2\Theta,$$

where $\mu_{xy}(E)$ and $\mu_z(E)$ are the absorption coefficients for $2s \rightarrow p_{xy}$ and $2s \rightarrow p_z$ dipole transitions, respectively, at energy E. The absorption coefficient for an allowed transition depends not only on the joint density of states but also on the electric dipole matrix element between initial and final states. Since the initial states are core levels, they only overlap with the final wavefunction within the core region. However, since our energy band calculations are carried out within the pseudopotential formalism, the pseudo-wavefunctions for the final states are least accurate within the core radius. Thus we are not able to perform accurate calculations for the absorption coefficient. For this reason, it is not possible to assign a value to the minimum degree of hybridization between Cs and C states which will result in a detectable structure in the spectra. Nevertheless, partial band structures given in Section III can be used to identify origins of the structures in the measured spectra.

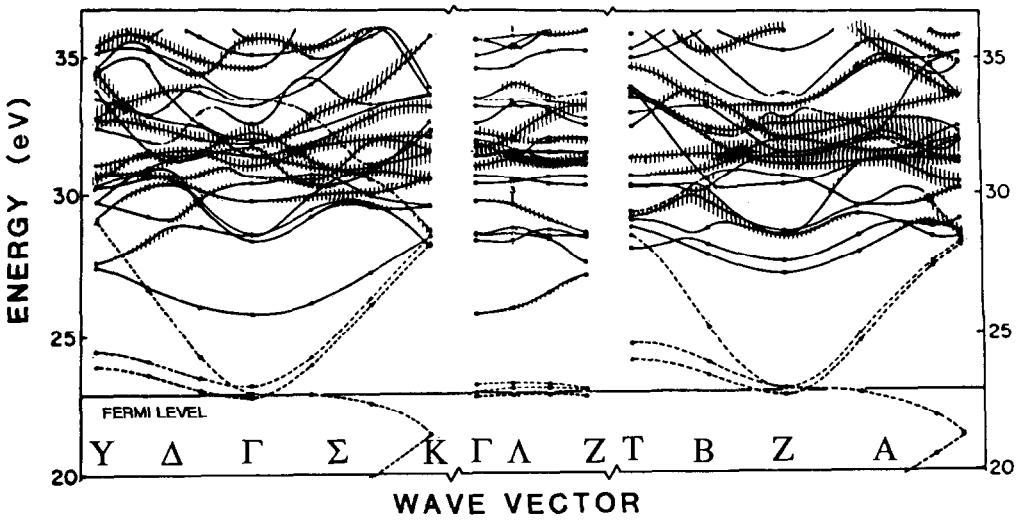

FIG. 5. Partial energy band structures of CsC_8, showing d content of the unoccupied states at the Cs site. Heights of the shaded areas are proportional to the sum of all the d components of the wavefunctions.

Figure 6 shows the measured spectra of CsC_8 for polarization angles varying between 30° and 90° in 15° steps. The peak marked A reduces in intensity and eventually disappears as the polarization angle Θ is reduced. This behavior indicates final states of p_{xy} symmetry. We identify it with transitions to a weak density of p_{xy} states about 1 eV above the Fermi level (Fig. 3). Even though their density is not high, they are observed since they do not overlap with any other strong transitions. The next peak is rather broad and strong and is composed of a primary peak B and a subsidiary structure B'. The latter appears only as a change of slope on the high energy side of B. These peaks are located about 6.1 and 9.5 eV beyond peak A and both become weaker as Θ is increased. However, they do not disappear completely for Θ = 90°, requiring large density of both p_{xy} and p_z states in this energy range. Indeed we find these states in the expected energy region, marked by arrows on the energy scale in Figs. 3 and 4. The next observed peak, close to 5740 eV, occurs at 20 eV above peak A and has the same behavior with polarization as the latter. It essentially disappears by the time Θ becomes 30°. Thus the final states for these transitions are almost exclusively of p_{xy} character. Our calculated energy band

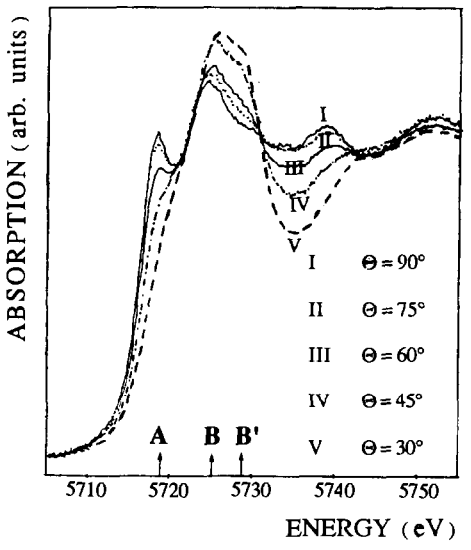

FIG. 6. Measured L_1 spectra of CsC_8 for values of polarization angle Θ from 30° to 90° by 15° steps.

structure indicates a large concentration of p_{xy} states at about 42 eV, i.e., about 18 eV above the region identified with peak A. There is essentially no state with p_z symmetry in this range. This region is not shown in Figs. 3–5 since the large number of bands beyond 35 eV would have rendered the figures incomprehensible.

Figure 7 shows the measured spectra for the second stage compound, CsC_{24}. The sequence of peaks, as well as their behavior as a function of polarization for stage 2 closely correspond to that of stage 1. The subsidiary peak B′ is essentially covered by B and is not observable in the second stage. Furthermore, the peak, observed at 5740 eV in the CsC_8 spectrum, appears less distinct in this case, possibly due to a larger overlap with the next structure on the high energy side. Figure 8 shows the measured spectra at $\Theta = 90°$ for stages 1 to 3. As expected, the spectra for the first two stages are quite similar in terms of the position of the peaks. The situation is, however, different for the third stage, where a broad peak replaces the

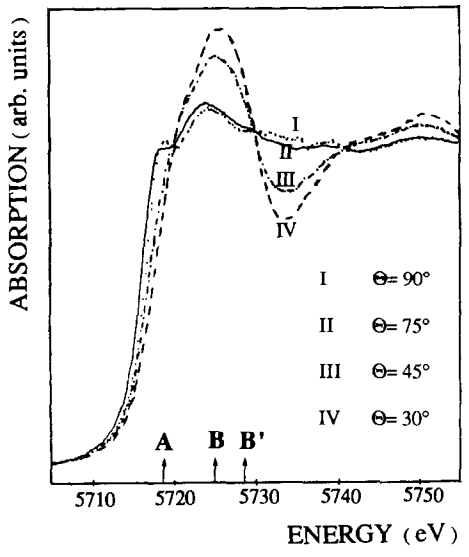

FIG. 7. Measured L_I spectra of CsC_{24} for values of polarization angle Θ from 30° to 90° by 15° steps.

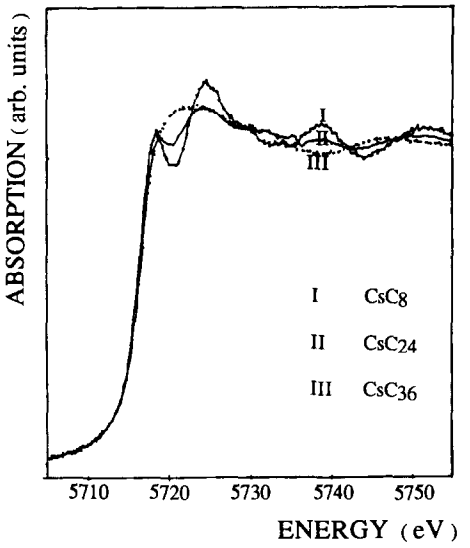

FIG. 8. Measured L_I spectra of first, second, and third stages of Cs GICs for polarization angle Θ of 90°.

first two. Based on the stoichiometry, one expects less change in going from the second to the third stage than from the first to the second. This was in fact the case for potassium GICs (*1*). We are, so far, unable to explain this anomaly in the results for the third stage, especially since the measured L_{II} and L_{III} spectra on these samples show very little change in shape and position of the peaks as a function of the stage (Fig. 11).

It is interesting to note that a narrow structure appears on the low energy side of the peak corresponding to B, in the K spectra of potassium GICs. The final states for this peak are due to hybridization of the potassium unoccupied p states with a set of flat bands between Γ and Z, located about 6 eV above the Fermi level of KC_8. In the cesium case, the unoccupied p states are located at higher energy and, thus, hybridize with a band of the appropriate symmetry and high dispersion, between 28 and 30 eV along the Γ to Z direction (Fig. 4). These states overlap with the final states responsi-

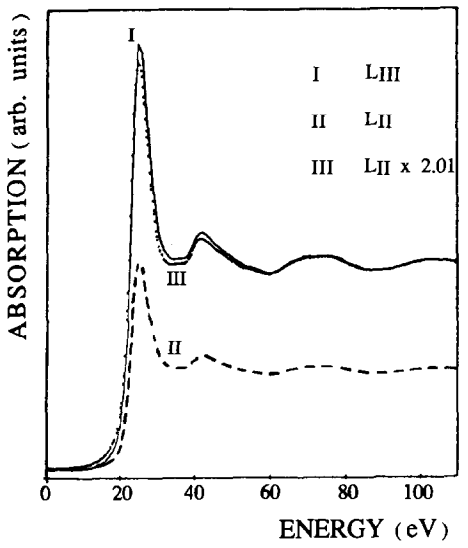

FIG. 9. Measured L_{III} and L_{II} spectra of CsC_8 for polarization angle Θ of 90°. The two spectra have been shifted so that the edges coincide in energy. Solid line represents the L_{III}, dashed line the L_{II}, and dotted line the L_{II} spectrum multiplied by a factor of 2.1.

ble for peak B and as a result the narrow structure is masked by this peak.

B. L_{II} and L_{III} Edges

L_{II} and L_{III} edges correspond to transitions from the $2p_{1/2}$ and $2p_{3/2}$ core levels of Cs, respectively. Selection rules allow transitions to final states with $\Delta l = \pm 1$ and $\Delta j = 0, \pm 1$ (*19*). Thus the final states for L_{II} edge are Cs $6s_{1/2}$ and $5d_{3/2}$ while for L_{III} the final states can be Cs $6s_{1/2}$, $5d_{3/2}$, and $5d_{5/2}$. Transitions to *s* final states are not normally observed due to both lower cross-section and the fact that they have a rather broad density-of-states.

Figure 9 presents the measured spectra for L_{II} and L_{III} edges for $\Theta = 90°$, shifted in energy such that the first peak positions coincide. Both spectra show strong, narrow absorption peaks at the edge. These are often observed in L_{II} and L_{III} edges of metals (*20–22*) and are referred to as *white lines*. They are attributed to either high density of final states or to excitons (*23, 24*). In our case, existence of final Cs *d* states, centered at about 9 eV above the Fermi level (Fig. 5), points to the former mechanism as the origin of the white lines. These states are distributed over a range of approximately 2–3 eV, which when convolved with the 3-eV width of the core level agrees well with the measured width of 5 eV. Since the spin–orbit splitting of the Cs $5d$ states is small (0.04 eV) compared to the band structure broadening of these states, we expect the final states to be an overlapping mixture of all the $5d$ states. Thus, the white lines are observed in both L_{II} and L_{III} edges, and are due to transitions to the same final states. If we assume the matrix elements for both transitions to be roughly the same, the ratio of L_{III} to L_{II} peak intensities should reflect the ratio of degeneracies of the core $2p_{3/2}$ to $2p_{1/2}$ levels, i.e., 2. Indeed, we find that if the L_{II} spectrum in Fig. 8 is multiplied by 2.1 it becomes indistinguishable from that of L_{III}.

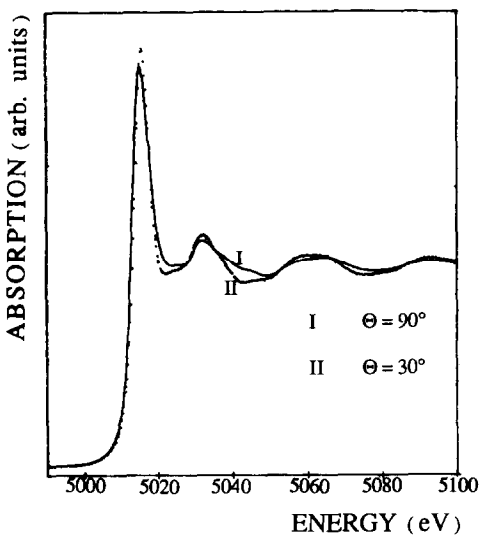

FIG. 10. Measured L_{III} spectra of CsC_8 for polarization angle Θ of 90° (solid line) and 30° (dotted line).

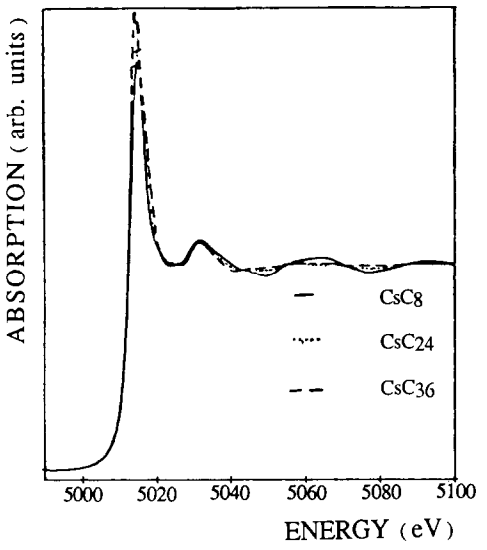

FIG. 11. Measured L_{III} spectra of first (solid line), second (dotted line), and third (dashed line) stages of Cs GICs for polarization angle Θ of 90°.

The same mixing of the 5 final *d* orbitals indicates that, in contrast to the L_I edge, L_{II} and L_{III} spectra of CsC_8 should not be very sensitive to the polarization angle of the incident beam. The measured L_{III} spectra (Fig. 10) in fact, confirm this conclusion. A similar behavior is observed for the L_{II} edge, not shown here.

Figure 11 gives the measured L_{III} spectra for the first three stages. We see very little differences in the shape and locations of the peaks for the three cases. This indicates that the final cesium *d* states which are located well above the Fermi level are, essentially, atomic like, with their positions shifted due to the transfer of charge from cesium to carbon layers. Coincidence of the L_{III} edges for the three stages indicates that the screening of cesium core levels due to charge transfer is the same in the three compounds (*1*). Since it is generally accepted that charge transfer in the second stage is unity, we can, therefore, conclude that, within experimental accuracy, it is also unity for the first stage. In fact, if the charge transfer was reduced by only 0.05 electron, the expected shift of the L_{III} edge, from atomic SCF calculations, will be about 0.3 eV. This is of the same order as the experimental resolution, setting the lower limit of 0.95 electron for the charge transfer from cesium to graphite. In the case of KC_8, a shift of 0.3 eV in the position of the K edge was used to obtain a 0.85 electron charge transfer. Thus such a large charge transfer between the intercalant and the graphite layer is a characteristic of all the heavy alkali GICs.

Acknowledgments

We thank Dr. A. C. Moore (Union Carbide) for providing the HOPG samples and we are indebted to Dr. R. Cortès for the use of data computing programs.

References

1. G. LOUPIAS, S. RABII, J. TARBÈS, S. NOZIÈRES, AND R. C. TATAR, *Phys. Rev. B* **41,** 5519 (1990).
2. A. HÉROLD, *Bull. Soc. Chim. France E,* 999 (1955).
3. A. MAAROUFI, S. FLANDROIS, AND D. GUÉRARD, *J. Chem. Phys.* **84,** 1443 (1987).
4. D. GUÉRARD, P. LAGRANGE, M. EL MAKRINI, AND A. HÉROLD, *Carbon* **6,** 285 (1978).
5. D. E. NIXON AND G. S. PARRY, *Br. J. Appl. Phys. Ser. 2* **1,** 291 (1968).
6. P. LAGRANGE, D. GUÉRARD, M. EL. MAKRINI, AND A. HÉROLD, *C.R. Acad. Sci. Sér. C* **287,** 179 (1978).
7. J. GOULON, R. CORTÈS, A. RETOURNARD, A. GEOGES, J. P. BATTIONI, R. FRÉTY AND B. MORAWECK, *Springer Proc. Phys.* **2,** 449 (1984).
8. J. GOULON, M. LEMMONIER, R. CORTÈS, A. RETOURNARD, AND D. RAOUX, *Nucl. Instr. Methods,* **208,** 625 (1983).
9. M. O. KRAUSE AND J. H. OLIVER, *J. Phys. Chem.* **8,** 329 (1979).
10. F. ROUSSEAUX, R. MORET, D. GUÉRARD, P. LAGRANGE, AND M. LELAURAIN, *Ann. de Physique,* **11,** 85 (1986); and F. ROUSSEAUX, R. MORET, D. GUÉRARD, AND P. LAGRANGE, *Phys. Rev. B* **42,** 725 (1990).
11. R. C. TATAR, Ph.D. Thesis, University of Pennsylvania (1985).
12. R. C. TATAR AND S. RABII *in* "Extended Abstracts (Fall Meeting of the Material Research Society)" (P. C. Eklund, M. S. Dresselhaus, G. Dresselhaus, Eds.), p. 71 (1984).

13. P. HOHENBERG AND W. KOHN, *Phys. Rev.* **136,** *B*864 (1964).
14. W. KOHN AND L. J. SHAM, *Phys. Rev.* **140,** *A*1133 (1965).
15. D. R. HAMANN, M. SCHLUTER, AND C. CHIANG, *Phys. Rev. Lett.* **43,** 1494 (1979).
16. L. HEDIN AND B. I. LUNDQVIST, *J. Phys. C* **4,** 2064 (1971).
17. S. G. LOUIE, K. M. HO, AND M. L. COHEN, *Phys. Rev. B* **19,** 1774 (1979).
18. M. SAITO AND A. OSHIYAMA, *J Phys. Soc. Japan* **55,** 4341 (1986).
19. L. F. MATTHEISS AND R. E. DIETZ, *Phy. Rev. B* **22,** 1663 (1986).
20. M. BROWN, R. E. PEIRELS, AND E. A. STERN, *Phys. Rev. B* **15,** 738 (1977).
21. F. SZMULOWICZ AND D. M. PEASE, *Phys. Rev. B* **17,** 334 (1978).
22. J. E. MULLER AND J. W. WILKINS, *Phys. Rev. B* **29,** 4331 (1984).
23. N. F. MOTT, *Proc. R. Soc. London* **62,** 416 (1949).
24. Y. CAUCHOIS AND N. F. MOTT, *Philos. Mag.* **40,** 1260 (1949).